

# Active Disturbance Rejection Control for Trajectory Tracking of a Seagoing USV: Design, Simulation, and Field Experiments

Jelmer van der Saag<sup>1,2</sup>, Elia Trevisan<sup>1</sup>, Wouter Falkena<sup>2</sup> and Javier Alonso-Mora<sup>1</sup>

**Abstract**—Unmanned Surface Vessels (USVs) face significant control challenges due to uncertain environmental disturbances like waves and currents. This paper proposes a trajectory tracking controller based on Active Disturbance Rejection Control (ADRC) implemented on the DUS V2500. A custom simulation incorporating realistic waves and current disturbances is developed to validate the controller’s performance, supported by further validation through field tests in the harbour of Scheveningen, the Netherlands, and at sea. Simulation results demonstrate that ADRC significantly reduces cross-track error across all tested conditions compared to a baseline PID controller but increases control effort and energy consumption. Field trials confirm these findings while revealing a further increase in energy consumption during sea trials compared to the baseline.

## I. INTRODUCTION

While oceans cover two-thirds of the Earth’s surface and approximately 37% of the global population resides within 100 kilometres of a shoreline [1], the ocean floor remains largely unmapped with only 15% coverage as of July 2019 [2]. Although still largely unexplored, the maritime domain remains critical for economic, scientific, and military advancements [3], underscoring the need for technological developments in marine exploration and navigation.

One such development has been the introduction of the Unmanned Surface Vessel (USV). These semi-autonomous vessels typically forgo an on-board crew, relying instead on a remote human operator or no operator at all. This shift significantly reduces crew requirements compared to traditional crewed vessels, resulting in lower operational costs and improved work safety, as an operator can remain in a safe environment [3]. Furthermore, the absence of a crew enables the design of smaller and more energy-efficient vessels, thus reducing their environmental footprint [4]. These benefits make USVs a suitable alternative to conventional vessels for a wide range of applications, including hydrographic surveys, offshore inspections, and maritime exploration [5], [6].

The maritime environment in which USVs operate can be particularly challenging due to environmental factors such as waves and currents. These disturbances are often unpredictable and negatively impact tasks such as trajectory tracking. Despite these challenges, path-following control has

This research is supported by the project “Sustainable Transportation and Logistics over Water: Electrification, Automation and Optimization (TRiLOGY)” of the Netherlands Organization for Scientific Research (NWO), domain Science (ENW), and the Amsterdam Institute for Advanced Metropolitan Solutions (AMS) in the Netherlands.

<sup>1</sup>Cognitive Robotics Department, TU Delft, 2628 CD Delft, The Netherlands , j.alonsomora}@tudelft.nl

<sup>2</sup>Demcon Unmanned Systems, Den Haag, 2583 WC, the Netherlands.

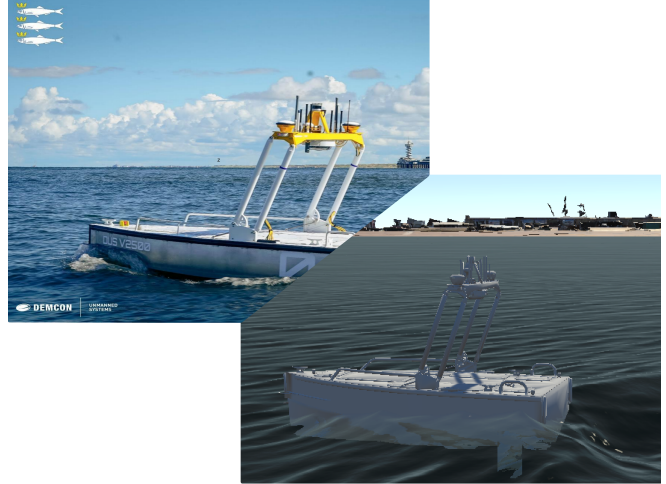


Fig. 1: DUS V2500 USV platform, operating near-shore in calm conditions in Scheveningen, the Netherlands (left) © Demcon Unmanned Systems. and in similar conditions in simulation (right).

often relied on traditional control methods, and Proportional-Integral-Derivative (PID) control remains the most popular approach in recent academic papers on USVs for its simplicity and ability to provide satisfactory performance [7]. However, PID control may struggle to maintain performance due to nonlinear system dynamics or rapidly changing environmental disturbances, leading to reduced performance in more challenging environments.

Various control strategies have recently been proposed to improve USV performance in dynamic environments. Alternatives to PID, such as Sliding Mode Control (SMC) [8], feedback linearisation [9], and backstepping control [10] have been widely applied [7]. However, these methods require varying degrees of system modelling, limiting their practicality in uncertain maritime conditions. Recent advances aimed at reducing this dependency include using neural networks to approximate unknown model dynamics [11] and techniques to replace system information with rapid measurements of state and disturbance estimation [12].

One technique aiming to eliminate model dependency, marketed as an extension to PID, is Active Disturbance Rejection Control (ADRC). It has seen adoption in USV control due to its ability to estimate uncertain system dynamics and external disturbances without any system information [13]. It allows for estimation of the “total disturbance” acting on the system, including internal uncertainties and external disturbances, which is compensated via a feed-forward component.

Although the effectiveness of ADRC in USV control has been repeatedly demonstrated in simulation studies [14]–

[19], real-world validations are limited. Existing experiments have been conducted only in inland waters [20], which lack significant disturbances such as stronger waves and currents. To the best of the authors' knowledge, no prior research has evaluated the performance of ADRC implemented on a seagoing USV through real-world testing.

We address this gap by designing and validating an ADRC-based control strategy on the DUS V2500, a fully electric USV developed by Demcon Unmanned Systems (DUS) as shown in Fig. 1. Capable of operating in conditions up to Sea State 4, the DUS V2500 is a suitable platform for evaluating ADRC performance in near-shore conditions. Performance is evaluated through simulation in a Unity environment featuring realistic waves and currents and field trials in Scheveningen, the Netherlands. Through these tests, we evaluate the feasibility of ADRC for seagoing applications. The contributions of this paper are as follows:

- The design and implementation of a trajectory-tracking second-order ADRC controller tailored for the DUS V2500, an underactuated, rudderless USV.
- The development and verification of a Unity-based simulation environment incorporating realistic wave, current, and wind disturbances to facilitate controller evaluation.
- The adaptation of a control strategy from quadrotor systems to a USV, addressing the challenges posed by propeller delay in an underactuated maritime platform.
- Real-world experimental validation of an ADRC controller for a USV at sea.

## II. PRELIMINARIES

This section provides an overview of the DUS V2500 platform, followed by a description of the system dynamics.

### A. USV Platform

The DUS V2500, as shown in Fig. 1, is a fully electric USV designed by Demcon Unmanned Systems for applications such as inspection and hydrography. The vessel measures approximately 2.5 metres in length and is primarily intended for inland and near-shore operations. It is rated to operate in conditions up to Douglas Sea State 4, corresponding to wave heights of up to 2.5 metres.

The platform is underactuated, featuring two stern-mounted thrusters and a single bow thruster for manoeuvring. The DUS V2500 operates without an onboard crew semi-autonomously, executing missions autonomously based on a predefined mission plan monitored by a remote operator.

The vessel's localisation is achieved through the fusion of Global Navigation Satelite System (GNSS) and Inertial Measurement Unit (IMU) data, providing estimates of the pose with an accuracy of  $\pm 0.01$  metres. A detailed description of the system architecture of the DUS V2500 is beyond the scope of this paper and remains proprietary to Demcon Unmanned Systems.

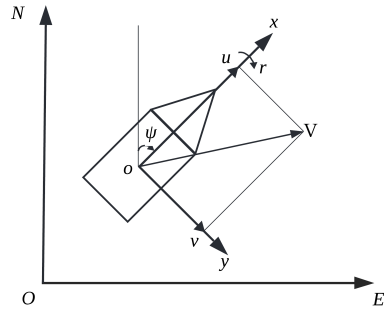


Fig. 2: Planar manoeuvring diagram of a USV where  $NOE$  denotes the geodetic NED coordinate system with  $O$  as the origin, and  $xoy$  denotes the body-fixed coordinate system with  $o$  as the USV's centre of gravity.  $V$  is the resulting velocity vector of  $u$  and  $v$ .

### B. System Dynamics

The dynamics of a ship are typically described in six degrees of freedom (DOF). For manoeuvring models, it is commonly assumed that the vessel is laterally and longitudinally stable, with negligible roll, pitch, and heave motion [21]. Under these conditions, the model reduces to a 3-DOF system described by the position and orientation vector  $\eta = [x, y, \psi]^T$  and the body-fixed velocity vector  $\nu = [u, v, r]^T$ , where  $(x, y)$  represents the Cartesian position,  $\psi$  is the yaw angle,  $(u, v)$  are the surge and sway velocities, and  $r$  is the yaw rate. Such a manoeuvring model is visualised in Fig. 2.

Accurately modelling the system requires identifying numerous hydrodynamic parameters that describe vessel dynamics. Studies have shown that even small discrepancies in sensitive parameters can lead to significant deviations in model predictions, adversely affecting control performance and trajectory tracking [22]. In addition, environmental disturbances such as wind, waves, and currents further complicate the modelling process. Accurate real-time estimation of such effects typically requires dedicated sensors for measuring free-stream air and water velocities or radar-based techniques for wave spectrum estimation [23]. These sensors are currently unavailable on the DUS V2500 platform, limiting its ability to predict environmental influences.

Due to these challenges, optimal control methods have seen limited adoption in USV control. Approaches with better robustness to uncertainties are often preferred [7].

## III. ACTIVE DISTURBANCE REJECTION CONTROL

This section first introduces the primary design principle behind ADRC, followed by an overview of a typical ADRC scheme and its essential components.

### A. ADRC Design Principle

As outlined in Sec. II, accurately modelling the system or the disturbances acting on it is a significant challenge. This limitation restricts the applicability of model-based control techniques in seagoing USVs, which are subject to considerable and often unpredictable disturbances. In contrast, ADRC reframes the problem by eliminating the need for precise knowledge of the system dynamics or disturbances. Instead, the unknown dynamics and external disturbances are seen as something to overcome by the control signal [13].

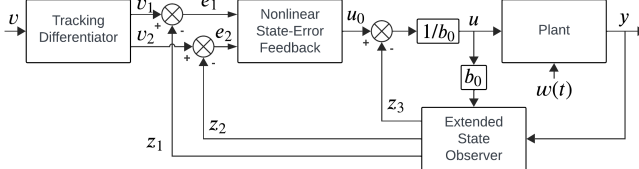


Fig. 3: Standard ADRC topology.

Consider a second-order system represented by the following equations:

$$\begin{cases} \dot{x}_1 = x_2 \\ \dot{x}_2 = F(t) + bu \\ y = x_1 \end{cases} \quad (1)$$

where  $y$  is the system output,  $u$  represents the input and  $F(t) = f(x_1, x_2, w(t), t)$  describes both the system states  $x_1$  and  $x_2$ , and disturbances  $w(t)$  as a function of time. Although  $F(t)$  may be unknown, the goal is to use the control effort  $u$  to compensate for it. In ADRC,  $F(t)$  is treated as an additional state variable, termed the “total disturbance” and denoted as  $x_3$ . This reformulates the original system as:

$$\begin{cases} \dot{x}_1 = x_2 \\ \dot{x}_2 = x_3 + bu \\ \dot{x}_3 = G(t) \\ y = x_1 \end{cases} \quad (2)$$

where  $G(t) = \dot{F}(t)$ .

### B. Basic ADRC Scheme

The standard ADRC scheme, as proposed by [13], comprises three primary components. These components are illustrated in Fig. 3 and are described in detail in the following subsection.

1) *Extended State Observer*: A state observer is constructed to estimate the total disturbance  $x_3$ . This observer, referred to as the Extended State Observer (ESO), is expressed as:

$$\begin{cases} e = z_1 - y \\ \dot{z}_1 = z_2 - \beta_{01}e \\ \dot{z}_2 = z_3 + b_0u - \beta_{02}\text{fal}(e, \alpha_1, \delta) \\ \dot{z}_3 = -\beta_{03}\text{fal}(e, \alpha_2, \delta) \end{cases} \quad (3)$$

where  $\mathbf{z}$  is the state observer’s estimate of  $\mathbf{x}$ ,  $\beta_{01}$ ,  $\beta_{02}$ , and  $\beta_{03}$  are the observer gains, and  $\text{fal}(e, \alpha, \delta)$  is a nonlinear function that replaces the proportional error  $e$  for  $z_2$  and  $z_3$  [13]. The function  $\text{fal}(e, \alpha, \delta)$  is defined as:

$$\text{fal}(e, \alpha, \delta) = \begin{cases} \frac{e}{\delta^{\alpha-1}}, & |e| \leq \delta \\ |e|^\alpha \text{sign}(e), & |e| > \delta \end{cases} \quad (4)$$

Here,  $\delta$  primarily determines the size of the linear region near the origin, while  $\alpha$  controls the linear region’s and nonlinear region’s slope for  $|e| > \delta$ . This nonlinear function is designed to improve convergence to the system state while minimising peaking, where the state estimation error

temporarily exhibits large transients due to high observer gains in response to sudden changes or disturbances [24]. The values of  $\alpha$  are typically set as  $\alpha_1 = 0.5$  and  $\alpha_2 = 0.25$  [13]–[15], with  $\delta$  remaining a user-defined parameter.

2) *Tracking Differentiator*: The Tracking Differentiator (TD) generates a transient profile that the system can reasonably follow to avoid sudden setpoint jumps. The ADRC scheme assumes an underlying second-order system, so a double integral plant can construct this profile. [13] proposes a discrete-time solution to such a double integral plant as:

$$\begin{cases} v_1 = v_1 + hv_2 \\ v_2 = v_2 + hu, \\ u = \text{fhan}(v_1 - v, v_2, r_0, h_0) \end{cases} \quad |u| \leq r \quad (5)$$

Where  $v_1$  and  $v_2$  are the transient state and state derivative, respectively,  $v$  is the controller setpoint,  $r$  is a parameter that can speed up or slow down the transient profile, and  $r_0$  and  $h_0$  are controller parameters. The discrete time-optimal solution  $\text{fhan}(v_1, v_2, r_0, h_0)$  can be written as:

$$\begin{cases} d = r_0 h_0 \\ d_0 = h_0 d \\ y = v_1 + h_0 v_2 \\ a_0 = \sqrt{d^2 + 8r|y|} \\ a = \begin{cases} v_2 + \frac{a_0-d}{2} \text{sign}(y), & |y| > d_0 \\ v_2 + \frac{y}{h}, & |y| \leq d_0 \end{cases} \\ \text{fhan} = - \begin{cases} r \text{sign}(a), & |a| > d \\ r \frac{a}{d}, & |a| \leq d \end{cases} \end{cases} \quad (6)$$

Per [13], this solution guarantees optimal convergence from  $v_1$  to  $v$  without overshoot when  $r_0 = r$  and  $h_0 = h$ . However, these parameters can be individually adjusted to change the tracking speed and smoothness of the transient profile, respectively.

3) *Nonlinear State Error Feedback*: Similar to the TD, the basic ADRC scheme proposes the use of the optimal solution to the double-integral plant,  $\text{fhan}(e_1, ce_2, r_1, h_1)$ , as a control law [13]:

$$\begin{cases} e_1 = v_1 - z_1 \\ e_2 = v_2 - z_2 \\ u_0 = \text{fhan}(e_1, ce_2, r_1, h_1) \\ u = \frac{u_0 - z_3}{b_0} \end{cases} \quad (7)$$

where  $c$  denotes the damping factor, an additional user parameter and  $b_0$  represents the control coefficient, which scales the magnitude of the control signal. This control law assumes that the underlying plant is a second-order system, as presented in Eq. 2, with the total disturbance  $z_3$  compensated for via a feed-forward term.

## IV. CONTROLLER DESIGN

The trajectory controller consists of three ADRC controllers operating in parallel, as shown in Fig. 4, one for each degree of freedom. Each ADRC controller has a topology

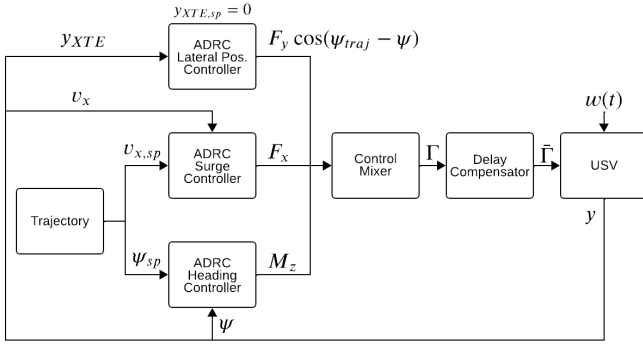


Fig. 4: Design of the trajectory-tracking controller using ADRC topology.

identical to that shown in Fig. 3. Although the dynamics of each degree of freedom are coupled, the effective decoupling performance of ADRC allows for individual control of each degree of freedom [19], [25].

The heading setpoint is derived from the trajectory using an L1 guidance law, which steers the USV towards the reference trajectory. The surge velocity is also derived from the trajectory and is set to the mission speed of 1.4m/s, automatically reducing during cornering to improve manoeuvrability. The setpoint of the lateral offset is fixed at zero, ensuring that the vessel follows the trajectory line. The output  $F_y$  of the ADRC lateral position controller is projected using the vessel's heading  $\psi$  and the trajectory line heading  $\psi_{traj}$ , ensuring  $F_y$ , and by extension  $F_B$ , primarily act when the USV is aligned with the reference trajectory.

#### A. Control Mixer

The control mixer translates the surge force  $F_x$ , sway force  $F_y$ , and yaw moment  $M_z$  from the controllers into individual thruster commands. As the system is underactuated, multiple solutions exist; however, under the following assumptions, a unique solution can be derived:

- The bow thruster is used exclusively to control the vessel's lateral position, with torque being controlled using the stern thrusters.
- The stern thrusters, mounted at an inward angle of  $\alpha$ , have a negligible lateral force contribution ( $\sin \alpha \approx 0$ ).

Then, the control mixer is defined as:

$$\begin{cases} F_{SL} = \frac{1}{2 \cos \alpha} \left( F_x + \frac{M_z + F_y x_{BT}}{y_{ST}} \right) \\ F_{SR} = \frac{1}{2 \cos \alpha} \left( F_x - \frac{M_z + F_y x_{BT}}{y_{ST}} \right) \\ F_B = F_y \end{cases} \quad (8)$$

where  $F_{SL}$ ,  $F_{SR}$ , and  $F_B$  represent the thrusts of the left stern thruster, right stern thruster, and bow thruster, respectively. The parameters  $x_{BT}$  and  $y_{ST}$  are geometric dimensions of the USV, denoting the longitudinal distance from the centre of mass to the bow thruster and the lateral distance to the stern thrusters, respectively.

#### B. Delay Compensator

Thruster speed changes are subject to spin-up and spin-down delays due to rotational inertia and propeller drag. A first-order low-pass filter can approximate this delay [26]:

$$\Omega(s) = \frac{\Omega_0(s)}{1 + s\tau_d} \quad (9)$$

where  $\Omega(s)$  denotes the actual thruster speed,  $\Omega_0(s)$  is the setpoint, and  $\tau_d$  represents the time constant, approximated as  $\tau_d = T_s/4$  [27].

For the DUS V2500, identified settling times are approximately  $T_s \approx 2$  seconds for the stern thrusters and  $T_s \approx 1$  second for the bow thruster, corresponding to time constants of  $\tau_d = 0.5$  and  $\tau_d = 0.25$  seconds, respectively. While not exact, this linear approximation suffices for delay compensation in ADRC [13], [26].

The delay compensator leverages the first-order approximation of the motor delay. For the total control signal  $\Gamma = [F_{SL}, F_{SR}, F_B]^\top$ , the delay is compensated using the following first-order approximation:

$$\bar{\Gamma} = \Gamma + \tau_d \dot{\Gamma} \quad (10)$$

where  $\bar{\Gamma}$  represents the compensated control signal,  $\dot{\Gamma}$  is the derivative of the control signal, and  $\tau_d = [0.5, 0.5, 0.25]^\top$  contains the time constants for the stern and bow thrusters.

The derivative  $\dot{\Gamma}$  is calculated using a separate Tracking Differentiator (TD) for each control signal. By setting a large value for  $r_0$ , the transient profile of the TD instantly adapts to changes in the input signal, effectively acting as a differentiation filter. This approach offers an improved noise tolerance [28] over numerical differentiation methods.

## V. SIMULATION DESIGN

A Software-In-The-Loop (SITL) simulation is used to validate the controller, comprising a digital twin of the onboard control computer integrated with a Unity-based simulation of vessel dynamics and sensor inputs. This simulation architecture, shown in Fig. 5, provides an environment for validating and evaluating controller performance under realistic operating conditions. An example of a USV in this simulation environment can be seen in Fig. 1.

This Unity simulation uses the Dynamic Water Physics 2 (DWP2) package to model vessel dynamics in six DOF [29]. Although a 3DOF manoeuvring model of the V2500 is available, based on system identification data, realistic simulation of environmental disturbances requires including roll, pitch, and heave dynamics. The DWP2 physics simulation is verified against an analytic manoeuvring model of the DUS V2500 with parameters identified from real-world data, as shown in Fig. 6. However, verification of the

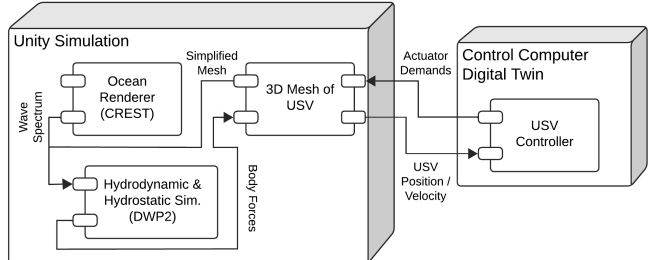


Fig. 5: Architecture of Unity Simulation.

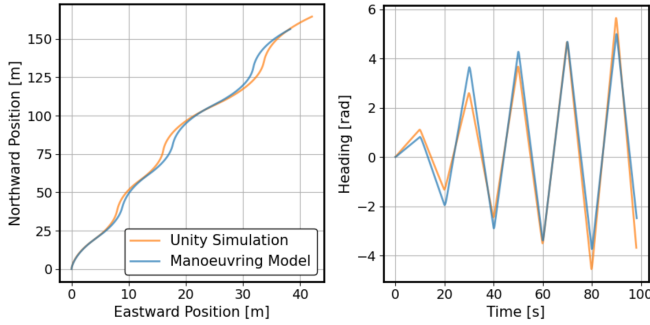


Fig. 6: Verification of the Unity simulation compared to a known manoeuvring model. The same thrust command sequences are fed to the vessel in our Unity simulator and an analytic manoeuvring model with parameters identified from data.

additional degrees of freedom (roll, pitch, and heave), which are primarily influenced by wave disturbances, is limited due to the absence of relevant system identification data or models. Collecting such data is costly, requiring wave tank experiments to establish known and precise wave conditions.

To simulate a realistic wave environment, DWP2 is integrated with the open-source CREST 4 ocean renderer, which generates a Pierson-Moskowitz wave spectrum [30]. The desired intensity of the wave spectrum can be easily specified to determine the total wave height, with sea states corresponding to Douglas Sea States 1-4 implemented within the simulation. This corresponds to a maximum wave height of 2.5m at sea state 4. Furthermore, CREST 4 supports fluid flow modelling, allowing the inclusion of ocean currents in the simulation.

## VI. SIMULATED EXPERIMENT

Simulated experiments are conducted to evaluate the performance of the ADRC controller against a baseline PID controller in a controlled environment. The experiment uses a predefined trajectory within the Derde Haven of Scheveningen, created with the navigation software stack developed by DUS. This software enables waypoint-defined trajectories that are compatible with both simulations and real-world testing.

The trajectory of the simulated experiment, shown in Fig. 7, consists of a combination of straight paths and corners, including acute turns and 90 degrees. Simulated disturbances, including waves and currents, originate from the north, as indicated by the white arrow in the figure. The trajectory is defined with a mission speed of 1.4 m/s. Dubins curves are used with a turning radius derived from the mission speed to ensure smooth transitions between segments. In simulation, the turning radius is set smaller than in real-world operations, as the physical limitations of the vessel are less restrictive. This adjustment enables the evaluation of more challenging trajectories, highlighting differences in controller performance more effectively.

Performance of both the ADRC controller and the baseline PID controller – currently deployed on the DUS V2500 – are evaluated using the same trajectory. The PID controller uses the gain values implemented in the production vessel, while the gains of the ADRC controller were manually

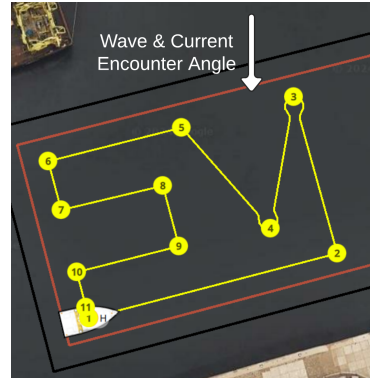


Fig. 7: In-harbour trajectory used for both simulated and real-world tests. The encounter angle for waves and currents applies only to the simulated experiment.

tuned for the experiment. Both controllers follow the control architecture depicted in Fig. 4, with the baseline replacing the ADRC controller with a standard PID controller.

Each controller is assessed in trajectory tracking under four distinct operating conditions:

- 1) No disturbances.
- 2) A current of 0.5m/s with no waves.
- 3) No current with sea state 4 waves (2.5m wave height).
- 4) Both a 0.5m/s current and sea state 4 waves.

The performance of the controllers is evaluated based on the following metrics:

- **Cross-Track Error (XTE):** The deviation from the desired trajectory.
- **Total Battery Usage:** The total battery capacity consumed (in Ampere-hours) by the USV, estimated by integrating the current delivered to each motor over the entire trajectory.

### A. Results

To evaluate the performance of each controller under varying conditions, five repetitions of the trajectory are conducted for each case to account for error margins. The Root Mean Square (RMS) of the XTE is computed over the length of each trajectory. This metric for each controller and condition is summarised in Fig. 8. Additionally, the total energy usage for each controller, averaged over 5 trajectories for each testing condition, is presented in Fig. 9.

A sample of the trajectories for both the ADRC and PID controllers, under conditions without disturbances and with

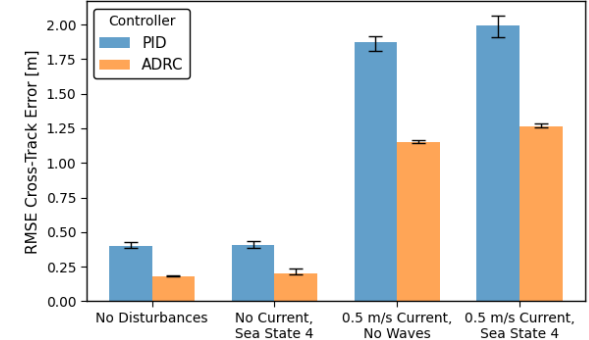


Fig. 8: RMS of the cross-track error (XTE) for each controller, averaged over 5 simulated trajectories. Error bars indicate min- and maximum values.

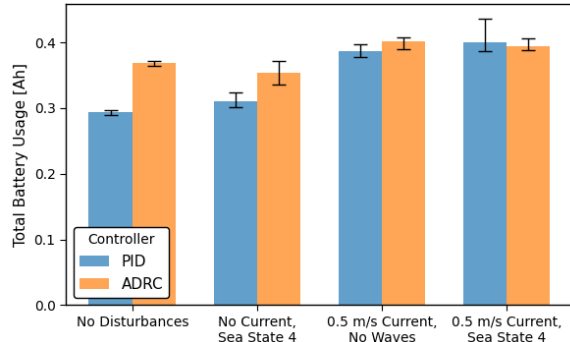


Fig. 9: Total battery consumption of each controller, averaged over 5 simulated trajectories. Error bars indicate min- and maximum measured values.

all disturbances active (0.5m/s current and sea state 4), is shown in Fig. 10.

### B. Discussion

The results demonstrate a clear performance improvement of the ADRC controller over the PID controller under all conditions. The ADRC controller achieves significant reductions in XTE, even in the absence of disturbances, indicating that the improved trajectory tracking is primarily due to the ADRC control law (Eq. 7) rather than its disturbance rejection capabilities.

As shown in Fig. 10, both controllers exhibit a constant lateral offset during straight-line tracking with currents. This offset results from the guidance law striving to align the vessel with the path. Only the bow thruster can compensate for the lateral offset in this configuration, but as it is not strong enough, its input saturates. Alternative guidance laws could also encourage using stern thrusters to correct the lateral offset, mitigating this effect.

Wave-induced disturbances have minimal impact on lateral error, with XTE remaining similar to no-wave conditions. Although slight trajectory variability is observed, it did not significantly affect overall tracking performance. This is likely due to limitations in the wave model, which may not fully capture wave-to-vessel momentum transfer. Despite increased pitch, roll, and heave motions, vessel manoeuvrability remained largely unaffected.

Battery consumption, illustrated in Fig. 9, is higher for the ADRC controller in calm conditions but comparable to the PID controller when exposed to currents. In the presence of current, ADRC demonstrates lower consumption by completing the trajectory quicker, as shown in Fig. 10.

The increased control effort of ADRC arises from the fundamental principle of counteracting  $F(t) = f(x_1, x_2, w(t), t)$  entirely through the control signal  $u$ , as defined in Eq. 2. This forces the system to behave as a second-order system, actively rejecting external disturbances and internal higher-order effects. However, since ADRC cannot distinguish between internal dynamics and external disturbances, its energy efficiency is inherently reduced.

## VII. REAL-WORLD EXPERIMENT

Field trials are conducted in two scenarios to evaluate the ADRC controller under varying environmental conditions.

The first scenario involves replicating the trajectory, defined by the same waypoints as in Fig. 10, within the controlled environment of Scheveningen Harbour, with minimal disturbances, as shown in Fig. 11.

The second scenario tests an identical trajectory in a near-shore environment outside the harbour to assess performance under increased wave and current disturbances, approximately 600 metres from the nearest groyne and 1 kilometre from the shore. An on-board view is shown in Fig. 11.

The gains and parameters for both controllers are kept identical to those used in the simulation, as they demonstrated satisfactory performance during field tests. This approach ensures a fair comparison between the controllers and highlights their ability to transfer effectively from simulation to real-world scenarios.

### A. Results

The weather conditions during the experiments are summarised in Tab. I based on meteorological data. This may differ slightly from local conditions; these could not be recorded due to the absence of required sensors. In-harbour tests are conducted under minimal disturbance, while sea trials are conducted in relatively calm weather. More challenging conditions were not available during our field experiments.

Identical metrics used in the simulation trials are applied to the field trials. Both the PID and ADRC controllers are evaluated on trajectories performed in the harbour and at sea. For each controller and location, two trajectories were recorded, resulting in a total of eight trajectories. The results, summarised in Fig. 12, present the XTE and the total battery usage. Both metrics were averaged over the two recorded trajectories.

### B. Discussion

The results of the real-world tests reveal trends similar to those observed in the simulation. As shown in Fig. 12, the ADRC controller achieves a reduction in XTE under all testing conditions, although this comes at the expense of increased battery consumption. However, the observed reduction in XTE is less pronounced than in simulation. As mentioned in Sec. VI, the turning radius could not be as sharp in the real world as in simulation as a safety precaution, which may have reduced ADRC's advantage over PID.

The most prominent result is the increased power consumption of the ADRC controller at sea. While a slight difference in battery usage is observed in the harbour, this difference is exacerbated at sea. We observed that the total disturbance estimate at sea would often spike, causing a spike

TABLE I: Experimental conditions of field trials.

Experiment	Condition	Magnitude	Direction
In Harbour	Sea State	0-1	N/A
	Wind Speed	6 kts	SSW
	Current Speed	N/A	N/A
At Sea	Sea State	1-2	N/A
	Wind Speed	8 kts	SSE
	Current Speed	0.7 kts	SSW

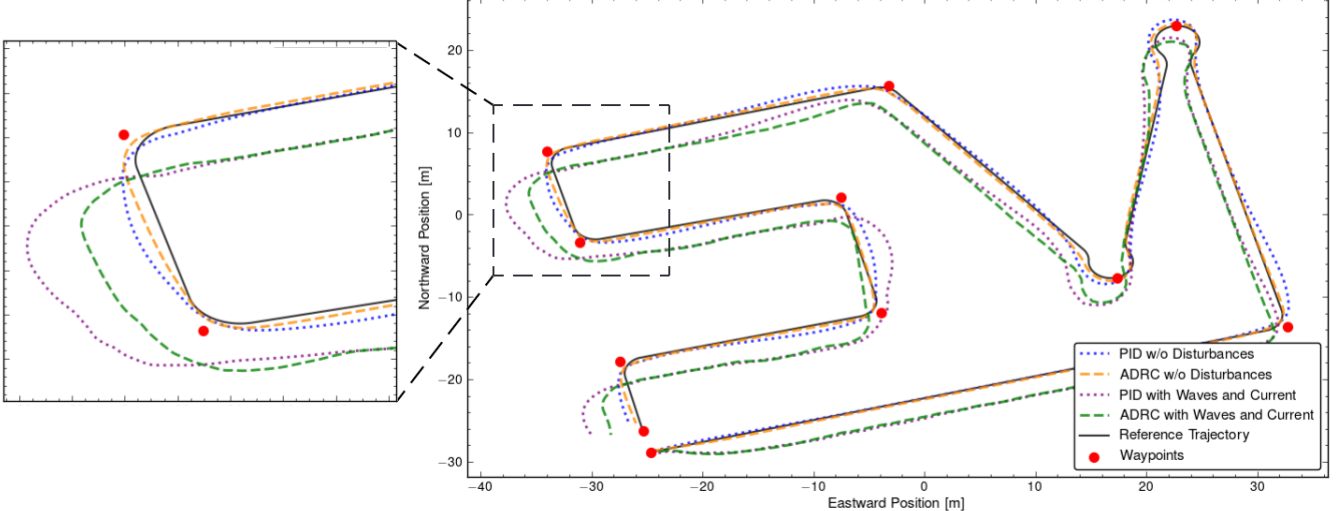


Fig. 10: Comparison of ADRC and PID controllers in simulation under different conditions. The steady-state error for both ADRC and PID in the presence of currents is due to input saturation on the bow thruster (see Eq. 8 and Subsec. VI-B).



Fig. 11: The DUS V2500 during in-harbour trials (left) and during near-shore trials (right) in Scheveningen, the Netherlands.

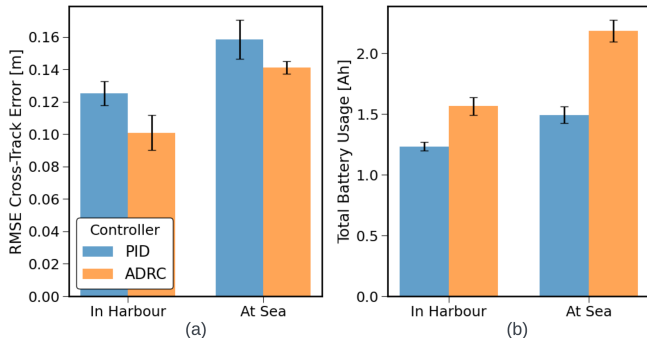


Fig. 12: (a) RMS of the cross-track error for each controller. (b) Total battery consumption of each controller. Both metrics are averaged over two measured trajectories. Error bars indicate the minimum and maximum measured values.

in torque demand as well. This is seen in Fig. 13, which causes the torque output to clip on hard limits.

This is a primary cause of the controller's inefficiency. As this total disturbance term includes internal and external effects, it cannot be clearly stated which effects are being overcompensated. However, it is clear that this feed-forward term that compensates the total disturbance  $z_3$  is excessive and should be scaled. To reduce excessive disturbance rejection, such modifications have been proposed [26].

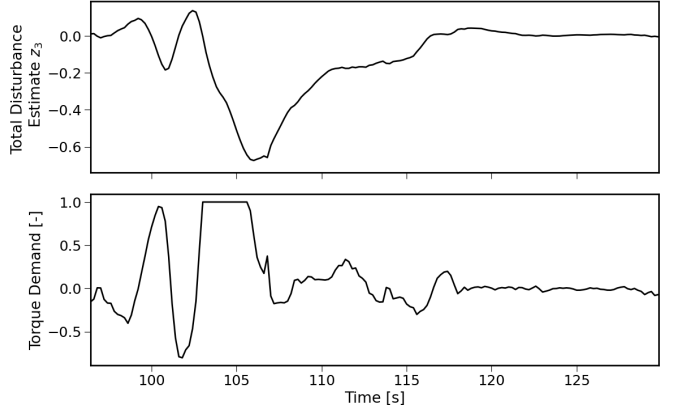


Fig. 13: Spike in the total disturbance estimate  $z_3$  during near-shore trials, resulting in torque saturation and increased power consumption.

## VIII. CONCLUSION

This study evaluates the performance of the ADRC framework for USV trajectory tracking through simulations and field trials. The results indicate that ADRC outperforms PID in reducing cross-track error in both simulation (by 30-40%) and field trials (by 10-20%).

In addition to the reduction in cross-track error, ADRC exhibits increased energy consumption compared to PID. In simulation, this increase is observed only in the absence of current. With currents present, ADRC completed the trajectory faster, resulting in equal battery usage. In field trials, the transition from harbour to near-shore conditions exacerbates this effect, with ADRC consuming approximately 50% more energy than PID.

In conclusion, while the ADRC controller enhances trajectory tracking, its increased energy consumption limits practical use in industrial USV applications. Future work should focus on optimising disturbance rejection by scaling the feedforward term and incorporating known system dynamics to better distinguish internal and external effects, thereby improving efficiency.

## ACKNOWLEDGMENT

This study would not have been possible without the generosity of Demcon Unmanned Systems, who provided their time and access to existing systems and software and made the V2500 available for testing in Scheveningen. A special thanks to the entire team for their invaluable support in preparing the vessel and assisting during the trials.

## REFERENCES

- [1] J. Yuh, G. Marani, and D. Blidberg, “Applications of marine robotic vehicles,” *Intelligent Service Robotics*, vol. 4, pp. 221–231, 10 2011.
- [2] J. H. Stel, *Exploring and Exploiting Deep Ocean Space*. Springer International Publishing, 2021, pp. 65–92.
- [3] Z. Liu, Y. Zhang, X. Yu, and C. Yuan, “Unmanned surface vehicles: An overview of developments and challenges,” *Annual Reviews in Control*, vol. 41, pp. 71–93, 2016.
- [4] V. Bolbot, A. Sandru, T. Saarniemi, O. Puolakka, P. Kujala, and O. A. Valdez Banda, “Small unmanned surface vessels—a review and critical analysis of relations to safety and safety assurance of larger autonomous ships,” *Journal of Marine Science and Engineering*, vol. 11, no. 12, 2023.
- [5] G. Roberts and R. Sutton, *Advances in Unmanned Marine Vehicles*. Advances in Unmanned Marine Vehicles, 01 2006.
- [6] *How USVs can Change the Offshore Inspection Market Through Novel Operating Models*, ser. OTC Offshore Technology Conference, vol. Day 1 Mon, May 06, 2024, 05 2024.
- [7] H. Xu and C. Guedes Soares, “Review of path-following control systems for maritime autonomous surface ships,” *Journal of Marine Science and Application*, vol. 22, pp. 153–171, 07 2023.
- [8] L. C. McNinch, H. Ashrafiun, and K. R. Muske, “Optimal specification of sliding mode control parameters for unmanned surface vessel systems,” in *2009 American Control Conference*, 2009, pp. 2350–2355.
- [9] E. Børhaug, A. Pavlov, E. Panteley, and K. Y. Pettersen, “Straight line path following for formations of underactuated marine surface vessels,” *IEEE Transactions on Control Systems Technology*, vol. 19, no. 3, pp. 493–506, 2011.
- [10] T. I. Fossen, M. Breivik, and R. Skjetne, “Line-of-sight path following of underactuated marine craft,” *IFAC Proceedings Volumes*, vol. 36, no. 21, pp. 211–216, 2003, 6th IFAC Conference on Manoeuvring and Control of Marine Craft (MCMC 2003), Girona, Spain, 17-19 September, 1997.
- [11] B. Qiu, G. Wang, Y. Fan, D. Mu, and X. Sun, “Adaptive course control-based trajectory linearization control for uncertain unmanned surface vehicle under rudder saturation,” *IEEE Access*, vol. 7, pp. 108 768–108 780, 2019.
- [12] W. Liu, H. Ye, and X. Yang, “Model-free adaptive sliding mode control method for unmanned surface vehicle course control,” *Journal of Marine Science and Engineering*, vol. 11, no. 10, 2023.
- [13] J. Han, “From PID to active disturbance rejection control,” *IEEE Transactions on Industrial Electronics*, vol. 56, no. 3, pp. 900–906, 2009.
- [14] J. Hu, Y. Ge, X. Zhou, S. Liu, and J. Wu, “Research on the course control of USV based on improved ADRC,” *Systems Science & Control Engineering*, vol. 9, no. 1, pp. 44–51, 2021.
- [15] F. Chen, H. Xiong, and J. Fu, “The control and simulation for the ADRC of USV,” in *2015 Chinese Automation Congress (CAC)*, 2015, pp. 416–421.
- [16] Y. Fan, L. Liu, and Y. Yang, “ADRC course control for USV based on fuzzy self-tuning,” in *2021 4th International Conference on Intelligent Autonomous Systems (ICoIAS)*, 2021, pp. 307–311.
- [17] Y. Zheng, J. Tao, Q. Sun, H. Sun, Z. Chen, M. Sun, and G. Xie, “Soft actor-critic based active disturbance rejection path following control for unmanned surface vessel under wind and wave disturbances,” *Ocean Engineering*, vol. 247, p. 110631, 2022.
- [18] M. Fu, Q. Wang, Y. Wang, and Y. Xu, “Design of ADRC for unmanned surface vehicle heading based on immune particle swarm optimization,” in *2021 IEEE International Conference on Mechatronics and Automation (ICMA)*, 2021, pp. 130–135.
- [19] H. Li, H. Chen, N. Gao, N. Aït-Ahmed, J.-F. Charpentier, and M. Benbouzid, “Ship dynamic positioning control based on active disturbance rejection control,” *Journal of Marine Science and Engineering*, vol. 10, no. 7, 2022.
- [20] D. Wu, K. Yuan, Y. Huang, Z.-M. Yuan, and L. Hua, “Design and test of an improved active disturbance rejection control system for water sampling unmanned surface vehicle,” *Ocean Engineering*, vol. 245, p. 110367, 2022.
- [21] R. Skjetne, Øyvind Smogeli, and T. I. Fossen, “Modeling, identification, and adaptive maneuvering of CyberShip II: A complete design with experiments,” *IFAC Proceedings Volumes*, vol. 37, no. 10, pp. 203–208, 2004, iFAC Conference on Computer Applications in Marine Systems - CAMS 2004, Ancona, Italy, 7-9 July 2004.
- [22] X.-G. Wang, Z. Zou, F. Xu, and R.-Y. Ren, “Sensitivity analysis and parametric identification for ship manoeuvring in 4 degrees of freedom,” *Journal of Marine Science and Technology*, vol. 19, 12 2014.
- [23] A.-A. Al-Habashneh, C. Moloney, and E. Gill, “Ocean wave spectrum estimation from marine radar data using the polar Fourier transform,” in *OCEANS 2014 - TAIPEI*, 2014, pp. 1–6.
- [24] B.-Z. Guo and Z. Zhao, *Active Disturbance Rejection Control for Nonlinear Systems: An Introduction*. John Wiley & Sons, 2016, pp. 93, 152.
- [25] Q. Zheng, Z. Chen, and Z. Gao, “A practical approach to disturbance decoupling control,” *Control Engineering Practice*, vol. 17, no. 9, pp. 1016–1025, 2009.
- [26] J. Zou, “Robust active disturbance rejection control scheme for quadrotor UAVs: Experimental prototyping,” Master’s Thesis, Eindhoven University of Technology, 8 2018.
- [27] N. S. Nise, *Control systems engineering*. John Wiley & Sons, 2020, pp. 163, 667.
- [28] J. Wang, H. Zhang, G. Xiao, Z. Dan, S. Zhang, and Y. Xie, “A comparison study of tracking differentiator and robust exact differentiator,” in *2020 Chinese Automation Congress (CAC)*, 2020, pp. 1359–1364.
- [29] “Dynamic Water Physics 2 Unity package,” <https://assetstore.unity.com/packages/tools/physics/dynamic-water-physics-2-147990>, accessed: 2025-02-27.
- [30] “CREST Unity package,” <https://github.com/wave-harmonic/crest>, accessed: 2025-02-27.